CHANGE DETECTION BASED ON PERSISTENT SCATTERER INTERFEROMETRY - CASE STUDY OF MONITORING AN URBAN AREA

C.H. Yang*, U. Soergel

Institute of Geodesy, Technische Universität Darmstadt, Germany - (yang, soergel)@geod.tu-darmstadt.de

KEY WORDS: Persistent Scatterer Interferometry (PSI), Change Detection, Urban Monitoring

ABSTRACT:

Persistent Scatterer Interferometry (PSI) is a technique to extract subtle surface deformation from sets of scatterers identified in time-series of SAR images which feature temporally stable and strong radar signal (i.e., Persistent Scatterers, PS). Because of the preferred rectangular and regular structure of man-made objects, PSI works particularly well for monitoring of settlements. Usually, in PSI it is assumed that except for surface motion the scene is steady. In case this is not given, corresponding PS candidates are discarded during PSI processing. On the other hand, pixel-based change detection relying on local comparison of multi-temporal images typically highlights scene modifications of larger size rather than detail level.
In this paper, we propose a method to combine these two types of change detection approaches. First, we introduce a local change-index based on PSI, which basically looks for PS candidates that remain stable over a certain period of time, but then break down suddenly. In addition, for the remaining PS candidates we apply common PSI processing which yields attributes like velocity in line-of-sight. In order to consider context, we apply now spatial filtering according to the derived attributes and morphology to exclude outliers and extract connect components of similar regions at the same time. We demonstrate our approach for test site Berlin, Germany, where, firstly, deformation-velocities on man-made structures are estimated and, secondly, some construction-sites are correctly recognized.

1. INTRODUCTION

Synthetic Aperture Radar (SAR) is a remote sensing technique providing radar images. Due to the active sensor principle and signal wavelength in centimeter scale, SAR is capable for night vision and independent from weather conditions, respectively. In addition, SAR may cover vast areas in short time with considerable fine spatial resolution (e.g., satellite TerraSAR-X, TSX, acquires in extreme case of Stripmap mode stripes of 30 *km* by 1500 *km* along orbit with geometric resolution of about 3 *m*). Therefore, in particular the techniques based on spaceborne SAR is widely used for tasks like monitoring and change detection. In this paper, we combine two established change detection methods based on SAR, which are complementary with respect to the kind of changes looked at, the exploited features, and the typical size of extracted results.

The first technique is called Persistent Scatterer Interferometry (PSI) (Ferretti et al., 2000; Ferretti et al., 2001; Ferretti et al., 2011; Hooper et al., 2004; Kampes, 2006), which aims at surface deformation by processing of time-series of SAR images. For this purpose the image stack is scanned for SAR resolution cells of temporally stable and strong radar signal that are called Persistent Scatterers (PS). PSI is an opportunistic geodetic approach, this means, on the one hand, we take advantage of PS no matter what object they cause or wherever they are located, but, on the other hand, the PS density can vary strongly and voids of considerable size frequently occur. Due to the preferred rectangular and regular structure of man-made objects, PSI works particularly well for urban areas. Subsequent PSI processing is conducted in a network of the identified PS set. After filtering of nuisances like atmospheric phase delay and thermal noise, by spatial-temporal double-differences of the signal phase, the relative motion in line-of-sight of the SAR sensors is obtained for each PS with respect to a reference PS. In order to avoid under-sampling, the relative PS-motion of two consecutive SAR images must neither temporally nor spatially exceed a 2π phase cycle (in case of TSX 1.5 *cm*). PSI has proven to be useful to monitor surface deformation in cities in the order of some millimeter per year (Crosetto et al., 2008; Gernhardt and Bamler, 2012; Perissin and Ferretti, 2007). Such deformation may be triggered by physical processes of various kinds leading to different motion behaviour such as linear long-term subsidence (Dixon et al., 2006; Liu et al., 2011; Osmanoğlu et al., 2011) or even sinusoidal pattern due to seasonal expansion of steel construction (Colesanti et al., 2003; Gernhardt et al., 2010; Monserrat et al., 2011) Even though a PS network is processed, standard PSI can be regarded as a local method because apart from post-processing like spatial low-pass filtering (e.g., according to a correlation length derived from some geophysical model of the underlying deformation process) the PS are essentially treated individually. And there is another limitation: Usually, in PSI processing it is assumed that except for surface motion the scene is steady: For instance, a building populated by certain substructures which produce some PS remains unchanged over the image stack. In case this is not true and such structures substantially alter or even vanish, corresponding PS candidates are discarded during PSI processing.

However, areas affected by bigger changes can be efficiently detected by the second common technique, we turn to now: pixel-based change detection applied to pairs or time-series of multi-temporal images. In the most basic approaches the grey values are directly compared, for instance, by image differencing, image rationing, or regression analysis (Hussian et al., 2013). No matter whether the amplitude, the coherence, or the differential phase of SAR images is used for analysis, noise

* Corresponding author.

might lead to undesired false alarms. Since noise is modelled to be spatially uncorrelated, such effect is mitigated by averaging preferably over connected image components. However, this inevitably comes along with loss of detail.

In this paper, we propose a method to combine these two types of change detection approaches. In Section 2, first we briefly outline PSI processing focussing on steps which are crucial for our further workflow. Based on this we introduce a local change-index derived from PSI, which basically looks for PS candidates that remain stable over a certain period of time, but then break down suddenly. In addition, for the remaining PS candidates we apply common PSI processing which yields features like velocity in line-of-sight. In order to consider context, we apply now filtering according to the derived attributes and morphology to exclude outliers and extract connect components of similar regions at the same time (Section 3). In short, the proposed method can determine two types of change instead of combining the results of PSI and pixel-based methods. In addition, we are able to combine attributes of PS-points (e.g. geographic coordinates) and extended features like regular grids of PS at façades in further applications. In Section 4, the approach is demonstrated for the example of the inner city of Berlin, Capital of Germany, where in the last decade many new buildings have been erected whereas others have been torn down.

2. CHANGE DETECTION BASED ON PERSISTENT SCATTERER INTERFEROMETRY

PSI requires a set of N multi-temporal SAR images taken from same orbit covering a study area. A master image is selected to pair with the other slave images to form $N-1$ interferograms. The optimal master image is chosen based on small-baseline constraint (Berardino et al., 2002; Lanari et al., 2004) to reduce the phase noise (caused by geometrical and temporal decorrelations) in the interferograms. The phases of pixels in interferograms (indicated by *p*) are expressed as

$$\phi^p(x) = \phi_r^p(x) + \phi_a^p(x) + \phi_n^p(x) \tag{1}$$

where x indicates pixel, $\phi_r^p(x)$ is the phase term related to the line-of-sight (LOS) distance between SAR sensor and target, $\phi_a^p(x)$ models the atmospheric phase component, and $\phi_n^p(x)$ is due to noise.

To determine the LOS-deformation-velocities (LOS will be omitted for simplicity) and the heights of PS-points, $\phi_r^p(x)$ can be decomposed into

$$\phi_r^p(x) = C_v^p(x)v(x) + C_h^p(x)h(x) \tag{2}$$

where $v(x)$ and $h(x)$ are the deformation-velocity and the height with respect to some point of reference, and $C_v^p(x)$ and $C_h^p(x)$ are the coefficients of $v(x)$ and $h(x)$, respectively. Hypothesize $v(x)$ is linear, $C_v^p(x)$ is expressed as

$$C_v^p(x) = \frac{4\pi}{\lambda} B_T^p \tag{3}$$

where λ is the wavelength of SAR signal, and B_T^p is the temporal baseline of interferogram. $C_h^p(x)$ is expressed as

$$C_h^p(x) = \frac{4\pi}{\lambda} \cdot \frac{B_\perp^p(x)}{r(x)\sin\theta(x)} \tag{4}$$

where $B_\perp^p(x)$ is the normal baseline of the interferogram, $r(x)$ is the LOS distance between SAR sensor and target, and $\theta(x)$ is the local incidence angle based on reference ellipsoid. To reduce the unknown range in estimating $h(x)$, the topography-height $h_{topo}(x)$ is subtracted from $h(x)$ to obtain residual-height $\Delta h(x)$ (In this paper, $h_{topo}(x)$ was provided by ASTER Global Digital Elevation Model, ASTER GDEM, in this paper). In short, $C_v^p(x)$ and $C_h^p(x)$ can be calculated from system parameters of the SAR sensor. Subsequently, $\phi^p(x)$ is the phase observation for solving the unknown $v(x)$ and $\Delta h(x)$ in the following Periodogram.

The estimated $\hat{v}(x)$ and $\Delta\hat{h}(x)$ are obtained by the Periodogram often called temporal coherence (Ferretti et al., 2001)

$$\arg\max_{v(x),\Delta h(x)} \left\{ |r| = \left| \frac{1}{N-1} \sum_{p=1}^{N-1} e^{j\left(\phi^p(x) - C_v^p v(x) - C_h^p \Delta h(x)\right)} \right| \right\} \tag{5}$$

where high ensemble temporal coherence $|r|$ indicates high accuracy of estimation, j is $\sqrt{-1}$, and the searching ranges and iteration-increments for $v(x)$ and $\Delta h(x)$ depend on a priori information. In addition, temporal coherence also reflects the phase stability of a pixel through the whole multi-temporal SAR image stack. Consequently, PS-points are selected if their temporal coherences are higher than a threshold (0.75 was used in this paper as empirical value). The choice of the threshold is a trade-off between accuracy of estimated unknowns and amount of PS-points. In urban areas, this threshold can be set higher because dense PS-points are expected anyway.

To increase the accuracy of $\hat{v}(x)$ and $\Delta\hat{h}(x)$, a second estimation step is implemented by Periodogram (5) after the estimated $\hat{\phi}_a^p(x)$ is removed from $\phi^p(x)$. Based on (1) and (2), $\phi_a^p(x)$ can be expressed as

$$\phi_a^p(x) = \phi_{res}^p(x) - \phi_n^p(x) \tag{6}$$

where the residual phase $\phi_{res}^p(x)$ is modelled as

$$\phi_{res}^p(x) = \phi^p(x) - C_v^p\hat{v}(x) - C_h^p\Delta\hat{h}(x). \tag{7}$$

Term $\phi_a^p(x)$ is assumed to be temporally uncorrelated and spatially correlated (Ferretti et al., 2000; Ferretti et al., 2001; Hooper et al., 2004). Thus, $\hat{\phi}_a^p(x)$ is obtained from $\phi_{res}^p(x)$

by using a spatiotemporal filter which consists of low-pass filter in space and high-pass one in time. In summary, the accuracy in second estimation can be improved because the atmospheric interferences have been diminished in the phase observations.

2.1 Change Index

In order to carry some PS-point, the underlying structure must not undergo any changes other than LOS-motion for the entire period of time spanned by PSI processing; else the PS candidate is most probably sorted out. This means, any "big change" (BC), for instance, demolition or construction of a certain building, occurring in the considered lapse of time almost inevitably comes along with loss of PS for the entire site of change. However, for a certain shorter period of time there might be PS found from the first SAR image to the event of demolition or from the end of construction to the last image, respectively. In order to identify such events, we run two PSI processing steps to be compared later. Firstly, in the I-PSI case we process the entire SAR image set (I- indicates "inclusive of big change"). PS candidates which undergo any big change are assumed to be discarded due to low temporal coherences $\left|r^{\mathrm{I}}(x)\right|$. Secondly, the F-PSI ("free of big change") case consists of a certain temporal sub set of SAR images without any big change. The temporal coherences $\left|r^{\mathrm{F}}(x)\right|$ of points accordingly should not be affected by appearing or vanishing objects. In short, $\left|r^{\mathrm{I}}(x)\right|$ and $\left|r^{\mathrm{F}}(x)\right|$ should be close if no big change occurred; otherwise $\left|r^{\mathrm{I}}(x)\right|$ is expected to be smaller than $\left|r^{\mathrm{F}}(x)\right|$.

To retrieve BC-points, we introduce a change-index

$$\underset{[-1\sim+1\in R]}{\mathrm{CI}(x)} = \left|r^{\mathrm{F}}(x)\right| - \left|r^{\mathrm{I}}(x)\right| \tag{8}$$

to quantify the possibility of big changes. Absolute values of CI close to 1 indicate strong hints to such modifications. Accordingly, BC-points are selected if their change-indices exceed a threshold. As a result, these BC-points are marked as big changes in a deformation-velocity image (I-PSI case) to form a new-style of change detection image (CD-image).

The city of Berlin still undergoes frequent activities in terms of renewal and construction of infrastructure, business districts, and residential buildings. In this paper, an area of the town is investigated where several buildings have been torn down recently (Figure 1). All PS-points in the F-PSI case are selected as BC-points if their change-indices exceed 0.3. At the time being this threshold was set manually. It may depend on many factors, for example, the number of SAR images and the a priori probability of big changes. The correlation between change-index and big changes will be explored in depth in future work.

3. OUTLIER-FILTERS

There are several causes of outliers such as: noise in phase observations, misfit of linear deformation-velocity hypothesis, inaccuracy of the topography-height model, inappropriate sampling of the Periodogram, under- or overestimated atmospheric phase item, and suboptimal setting of thresholds applied for extracting PS- and BC-points. Three types of outlier are described below as well as their corresponding removal strategy. All filters are designed based on sliding-window operation.

Isolated outliers: We deal with objects like buildings, industrial plants and infrastructure of a certain minimal size. Therefore, we remove PS- or BC-point which are isolated inside a 5 x 5 pixel sliding window.

Inconsistent outliers: One type of point will emerge as an outlier when it is surrounded mostly by heterogeneous points as connected components are expected to comprise single object. For example, in practice, a PS-point is unlikely to last when a construction event (full of BC-points) covers it. The PS- or BC-points are removed if their amount within a 3 x 3 window is less 3.

PS-points with peculiar velocity estimates: A PS-point whose deformation-velocity is implausibly large or is singular compared with the other neighboring points is recognized as outlier. Two filters are developed here. Firstly, a PS-point is removed as outlier if its deformation-velocity exceeds the tolerance range: -2 to +2 (*mm/year*). Secondly, the average of and standard deviation of deformation-velocities are calculated within a 3 x 3 window. Then the center PS-point is deleted if the difference between its deformation-velocity and the average exceeds 0.5 *mm/year* or 3-multiple of the standard deviation.

4. RESULTS AND DISCUSSION

4.1 Materials and Study Area

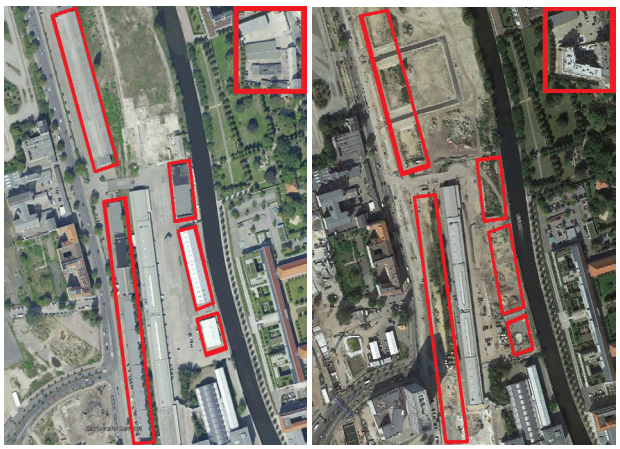

(a) 2010.09.12 (b) 2014.09.05

Figure 1. Study area (0.3 km^2) near the north of Berlin Central Station, Berlin. (a) Google-Earth image taken on 2010.09.12; (b) Google-Earth image, 2014.09.05. Red rectangles: construction-sites (the original buildings have been demolished but reconstruction if any is still in preparation stage).

In this experiment, we generated a CD-image presenting the construction-sites and deformation-velocities of steady buildings over Berlin. A cut-out from this image is used as the study area (Figure 1) in this paper. Here, the type of modification is restricted to demolished buildings. The construction-sites (Figure 1) are confirmed by using Ground truth in form of six historic images available in Google Earth. They have been taken in the acquisition period of the forty TSX-images (from 2010.10.27 to 2014.09.04). These images are used in the I-PSI and F-PSI cases. The ground resolution is resampled into 1 *m*.

In order to compare with pixel-based approaches, ratio and coherence-difference images are calculated (Figures 2(a, b)). They are generated based on (Rignot and van Zyl, 1993) and (Liu et al., 2001), respectively. Although the construction-sites can be at least partly recognized by naked eye, ubiquitous image noise renders any automatic pixel-based change detection to be very hard or even impossible.

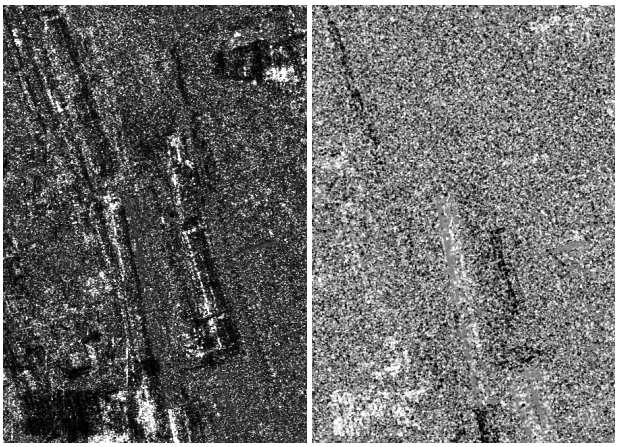

(a) Ratio image (b) Coherence-difference image

Figure 2. Pixel-based change images. (a) Ratio image (ratio of first TSX-image (2010.10.27) to last one (2014.09.04)). (b) Coherence-difference image (subtract first coherence image from second one). First coherence image is generated from two TSX-images taken on 2010.10.27 and 2013.08.15; Second coherence image, 2013.08.15 and 2014.09.04. In both images white or black pixels indicate changes (i.e., large difference).

4.2 Results of PSI Processing

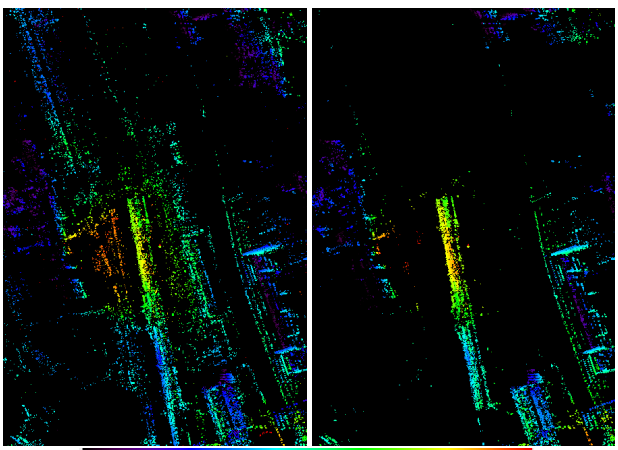

(a) (b)

Figure 3. (a) 24937 PS-points in F-PSI case; (b) 14652, I-PSI case. The height of the PS relative to the ASTER GDEM is coded in false color.

The I-PSI stack consists of the entire set of forty TSX-images in which the construction-sites (Figure 1) were captured. All demolished buildings have been torn down after the sixteenth TSX-image (2012.02.12) was acquired. Thus, the F-PSI case comprised these first sixteen TSX-images only to avoid degrading temporal coherences of points due to ongoing construction activities.

The PS-points (Figure 3) in the F-PSI and I-PSI cases show good agreement with the shape of the buildings. We observed that 10285 PS-points on the construction-sites in the F-PSI case (Figure 3(a)) disappear in the I-PSI case (Figure 3(b)). Due to thresholding according to the temporal coherence value, the noise prone regions visible in Figure 2(a, b) are mostly suppressed now. This enables to continue the analysis by a sequence of low-level image processing methods which are described in more detail below.

4.3 Change-index Image

The change-index image (Figure 4) is generated by subtracting the temporal coherence image in I-PSI case from the one in F-PSI case. Generally, the change-indices of points on the construction-sites (Figure 1) exceed 0.3. Thus, such points tend to show up in yellow or red in the false-color change-index image. On the contrary, the points on the steady buildings have change-indices near to 0 indicated by light-green. Otherwise, the remaining points appear as noise-like pattern if they are not located on buildings. In short, we observe that from the change-index image construction-sites can be discriminated from endured buildings. Their positions and outlines are clearer visible compared to the ones in the ratio and coherence-difference images (Figures 2(a, b)).

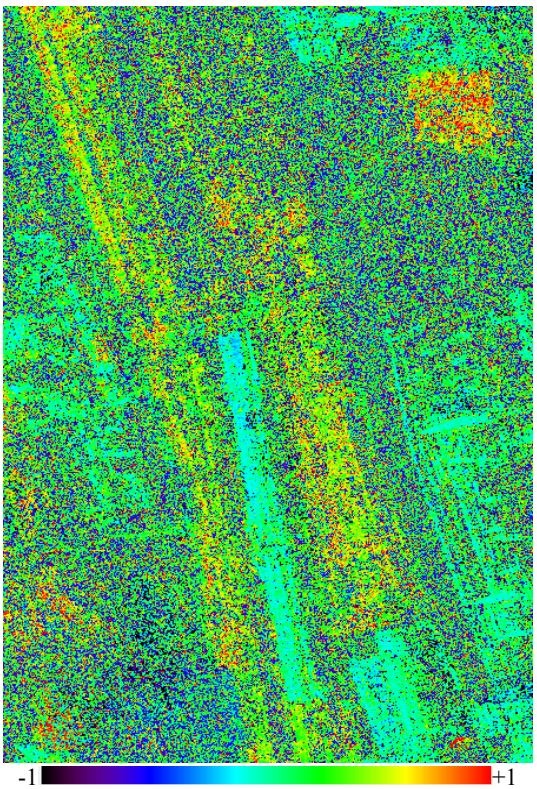

Figure 4. Change-index image. Color table: change-index.

The 5318 BC-points (Figure 5) are extracted from the PS-points in F-PSI case (Figure 3(a)) if their change-indices are equal to or above 0.3. We observe that the number of these BC-points (5318) is less than the one of the disappeared PS-points (10285, Figure 3). In our opinion this mainly is due to the following reason. Instead of relying on a global hard threshold we use a relative measure which is more appropriate to adapt to local conditions. For example, a certain façade may be populated by small sub-structures that provide only weak PS-points. In such case we deal with stable signal of however moderate temporal coherence only. Hard thresholding might result in entire loss of such structure. This is avoided by the index which provides a

relative measure. Nevertheless, the threshold of 0.3 ensures that we yield only significant BC-points.

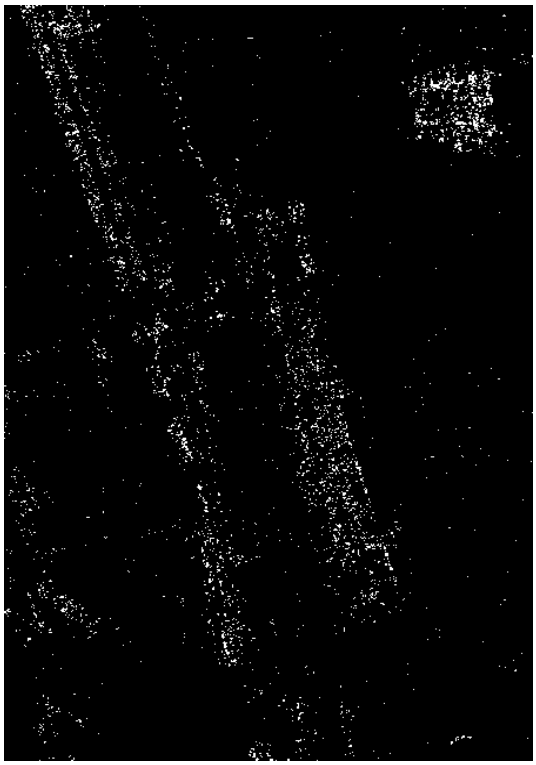

Figure 5. 5318 BC-points extracted from change-index image (Figure 4).

Overall, the positions of most BC-points (Figure 5) correspond to the construction-sites (Figure 1). However, we also recognize the noise-like BC-points (outliers) which need to be removed by the outlier-filters in the following steps.

4.4 New-style Change-detection Image

The new-style CD-image (Figure 6) is generated by adding the BC-points (Figure 5) to the deformation-velocity image (I-PSI case). This CD-image presents both the construction-sites (indicated by BC-points) and the deformation-velocities of steady buildings (indicated by PS-points). The positions of most BC-points are consistent with the construction-sites (Figure 1). In contrast to BC-points, PS-points are located on the steady buildings. Their deformation-velocities are quite uniform, which indicates plausible results. Overall, the distribution of BC- and PS-points is consistent with Ground Truth (Figure 1). However, we observe three types of outliers which have to be filtered in the subsequent steps:

- The PS- and BC-points outside the buildings.
- The PS-points on the construction-sites.
- The BC-points on the steady buildings.

The filtered CD-image (Figure 7) is generated by applying the outlier-filters described in Section 4 to the initial CD-image (Figure 6). The 2921 outliers have been removed from the 12003 BC- and PS-points, whereas the construction-sites and the steady buildings are maintained.

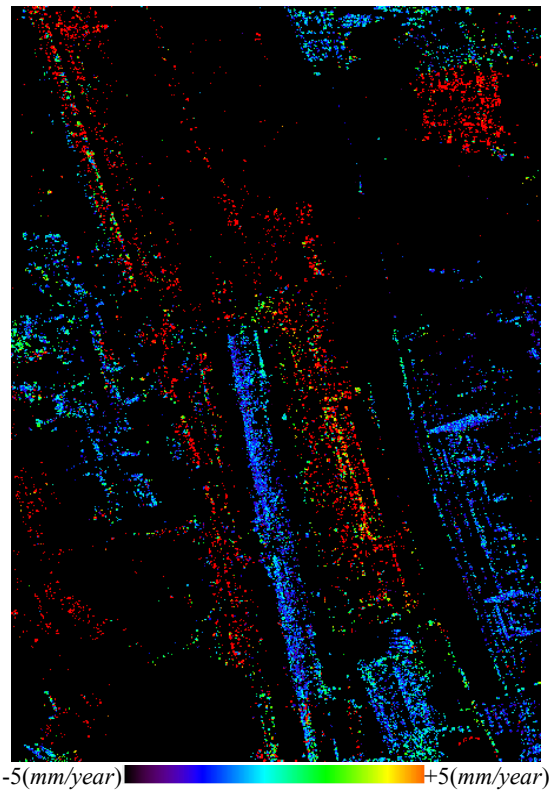

Figure 6. CD-image (before outlier-filterings). Color table, deformation-velocity of PS-point. Positive value in color table means deformation moves away from satellite; Negative value: towards. Red points: BC-points.

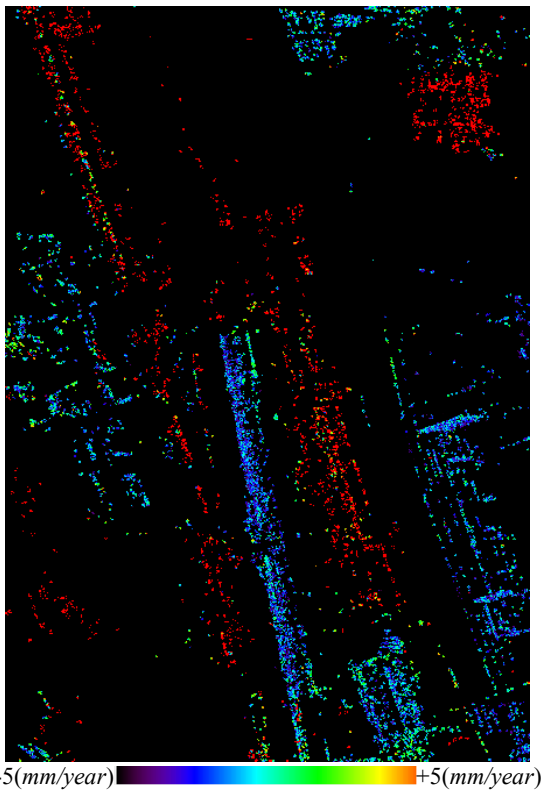

Figure 7. CD-image (after outlier-filterings). Color table, deformation-velocity of PS-point. Positive value in color table means deformation moves away from satellite; Negative value: towards. Red points: BC-points.

This contribution has been peer-reviewed.
Editors: U. Stilla, F. Rottensteiner, and S. Hinz
doi:10.5194/isprsarchives-XL-3-W3-123-2015

Three examples of outlier removal are discussed now using the details of the filtered CD-image (Figure 7). In Figure 8 a cut-out is depicted that shows an area covered by deciduous trees and lawn. Usually, in such environment hardly any PS-point occurs. The few and scattered PS- and BC-point candidates, left after PSI processing, have been successfully removed in the filtered image. Figure 9 shows an example where false PS-points on the construction-site have been removed. Finally in Figure 10 the BC-points on the steady building have been removed. Since few outliers still remain, developing more sophisticated filtering methods is required in future work.

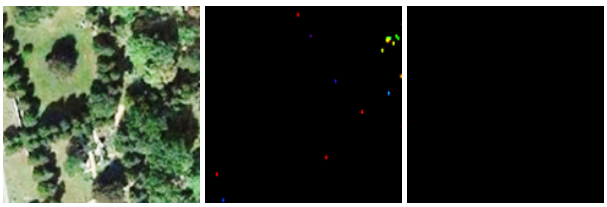

(a) (b) (c)

Figure 8. PS- and BC-points in vegetated area have been removed in filtered CD-image by outlier-filters. (a) Google-Earth image. (b) Cut-out of CD-image (Figure 6). (c) Cut-out of filtered CD-image (Figure 7). Non-red colors: PS-points, red: BC-points.

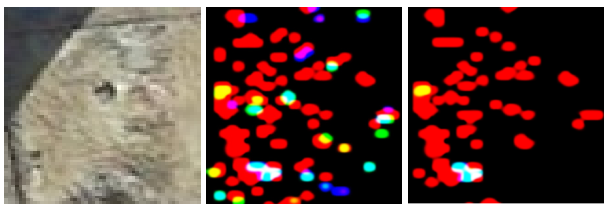

(a) (b) (c)

Figure 9. PS-points on construction-sites have been removed in filtered CD-image by outlier-filters. (a) Construction-site (Google-Earth image). (b) Cut-out of CD-image (Figure 6). (c) Cut-out of filtered CD-image (Figure 7). Non-red colors: PS-points, red: BC-points.

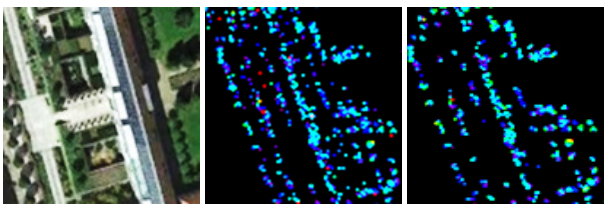

(a) (b) (c)

Figure 10. BC-points on steady buildings have been removed in filtered CD-image by outlier-filters. (a) Steady buildings (Google-Earth image). (b) Cut-out of CD-image (Figure 6). (c) Cut-out of filtered CD-image (Figure 7). Non-red colors: PS-points, red: BC-points.

In the lower left of Figure 7 we see some hints to changes highlighted in red not discussed so far. Comparing with Figure 1 we notice that some new buildings have been erected in this area. However, it is yet unknown when exactly these constructions took place, but it seems that those changes occurred at a later stage than those discussed so far. Also an image-by-image check of the entire SAR data stack did not provide more insight because of severe disturbance by noise even for the large building at the very bottom of the scene. Nevertheless, the change detection result reflects those changes at least to some extent.

4.5 Examples of Different Applications over Berlin

Here we demonstrate four examples to show the ability of the proposed method to monitor urban area. All of them are located in the inner city area of Berlin.

In the first example (Figure 11), the PS- and BC-points can be correctly recognized on steady buildings and construction-sites, respectively. The deformation-velocities on each building are homogeneous and therefore plausible. The sites with construction activities give rise to areas densely populated by BC-points.

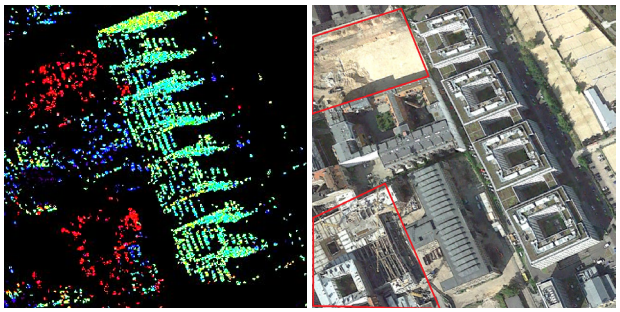

(a) (b)

Figure 11. Example of monitoring buildings. (a) Cut-out of filtered CD-image covering Berlin. Color table, shown in Figure 7. Non-red colors: PS-points, red: BC-points. (b) Cut-out of Google-Earth image (2014.09.05). Red polygons: construction-sites.

In Figure 12 the area around Berlin Central Station is presented. The big change of roof-structure of the building at the bottom right is detected in addition to the other construction-sites. Moreover, the outline of waterways can also be recognized. This finding implies that big change along waterway (e.g. flood or extension) can be detected by the proposed method. A further example (Figure 13) is related to a sports and recreation area including a stadium (Friedrich-Ludwig-Jahn-Sportpark). Fortunately, there is no undesired motion of the stadium itself; however we can clearly see big changes due to construction at the right wing of the hall in the upper part.

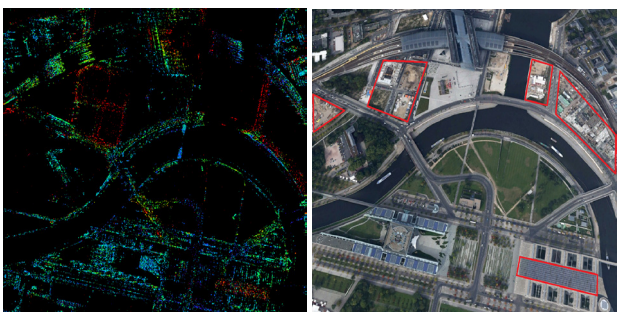

(a) (b)

Figure 12. Example of monitoring area around Berlin Central Station. (a) Cut-out of filtered CD-image covering Berlin. Color table, shown in Figure 7. Non-red colors: PS-points, red: BC-points. (b) Cut-out of Google-Earth image (2012.05.20). Red polygons: construction-sites.

Finally, an interesting case is shown in Figure 14 where two round areas are highlighted. The left one indicated by the red circle coincides with so called Marx-Engels-Forum, a former central square dedicated to communist leaders, which currently undergoes modification leading to BC-points. The right one

(blue circle) shows a monument called Neptunbrunnen located on an open place, where PSI indicates some LOS-motion of unknown origin.

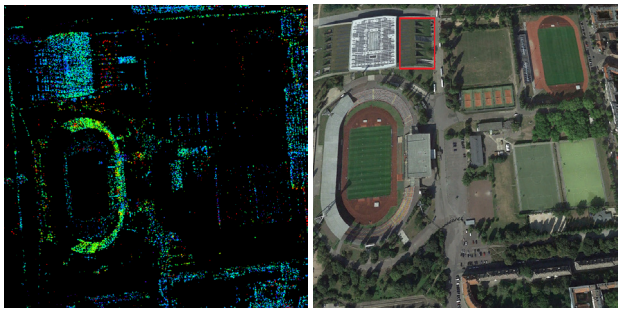

(a) (b)

Figure 13. Example of monitoring a stadium (Friedrich-Ludwig-Jahn-Sportpark). (a) Cut-out of filtered CD-image covering Berlin. Color table, shown in Figure 7. Non-red colors: PS-points, red: BC-points. (b) Cut-out of Google-Earth image (2014.09.05). Red rectangle: construction-site.

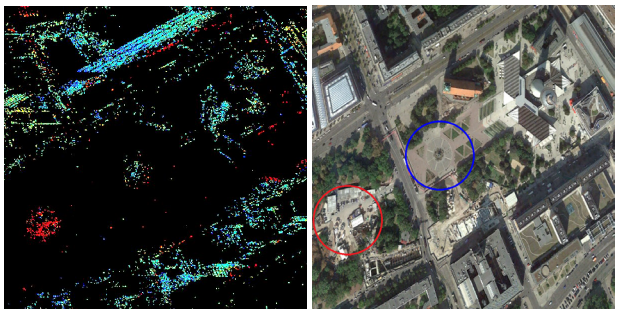

(a) (b)

Figure 14. Example of monitoring round areas. (a) Cut-out of filtered CD-image covering Berlin. Color table, shown in Figure 7. Non-red colors: PS-points, red: BC-points. (b) Cut-out of Google-Earth image (2014.09.05). Red circle: construction-site of Marx-Engels-Forum, blue circle: Neptunbrunnen.

5. CONCLUSIONS AND FUTURE WORK

We proposed a method to combine PSI and pixel-based change detection from a given stack of suitable SAR images. In this manner we are able to detect both changes at object level (e.g., emergence or vanishing of buildings) and surface deformation. By combining these two complementing processes we can get a richer picture of ongoing changes in urban areas.

The findings presented in this paper represent outcomes of our first experiments. Of course, there is still much room for improvement; for instance, we have set a few thresholds manually. In future work, these thresholds shall be set according to analysis of the given data and a priori knowledge about the scene. At the time being, we have selected the period of time assuming no big changes occurred (F-PSI stack) globally and manually for our test area. In order to work towards an operational approach, this has to be done in a smarter manner: Firstly, we need a local approach since construction activities in different quarters are usually not correlated. Secondly, we want to find the optimal temporal partition in a data driven manner. This means we have to run several PSI frameworks spanning different time lapse for F-PSI and to find the best set-up for a certain part of the scene.

REFERENCES

Berardino, P., Fornaro, G., Lanari, R. and Sansosti, E., 2002. A new algorithm for surface deformation monitoring based on small baseline differential SAR interferogram. *IEEE Trans. Geosci. and Remote Sens.*, 40(11), pp. 2375-2382.

Colesanti, C., Ferretti, A., Novali, F., Prati, C. and Rocca, F., 2003. SAR monitoring of progressive and seasonal ground deformation using the permanent scatterers technique. *IEEE Trans. Geosci. and Remote Sens.*, 41(7), pp. 1685-1700.

Crosetto, M., Biescae, E., Duro, J., Closa, J. and Arnaud, A., 2008. Quality assessment of advanced interferometric products based on time series of ERS and Envisat SAR data. *Photogramm. Eng. Remote Sens.*, 74(4), pp. 443-450.

Dixon, T. H., Amelung, F., Ferretti, A., Novali, F., Rocca, F., Dokka, R., Sella, G., Kim, S. W., Wdowinski, S. and Whitman, D., 2006. Subsidence and flooding in New Orleans. *Nature*, 441, pp. 587-588.

Ferretti, A., Prati, C. and Rocca, F., 2000. Nonlinear subsidence rate estimation using permanent scatterers in differential SAR interferometry. *IEEE Trans. Geosci. and Remote Sens.*, 38(5), pp. 2202-2212.

Ferretti, A., Prati, C. and Rocca, F., 2001. Permanent scatterers in SAR interferometry. *IEEE Trans. Geosci. and Remote Sens.*, 39(1), pp. 8-20.

Ferretti, A., Fumagalli, A., Novali, A., Prati, C., Rocca, F. and Rucci, A., 2011. A new algorithm for processing interferometric data-stacks: SqueeSAR. *IEEE Trans. Geosci. and Remote Sens.*, 49(9), pp. 3460-3470.

Gernhardt, S. and Bamler, R., 2012. Deformation monitoring of single buildings using meter-resolution SAR data in PSI. *ISPRS J. Photogramm. Remote Sens.*, 73, pp. 68-79.

Gernhardt, S., Adam, N., Eineder, M. and Bamler, R., 2010. Potential of very high resolution SAR for persistent scatterer Interferometry in urban areas. *Ann. GIS*, 16(2), pp. 103-111.

Hooper, A., Zebker, H., Segall, P. and Kampes, B., 2004. A new method for measuring deformation on volcanoes and other natural terrains using InSAR persistent scatterers. *Geophys. Res. Lett.*, 31(23), pp. 1-5.

Hussain, M., Chen, D., Cheng, A., Wei, H. and Stanley, D., 2013. Change detection from remotely sensed images: from pixel-based to object-based approaches. *ISPRS J. Photogramm. Remote Sens.*, 80, pp. 91-106.

Kampes, B. M., 2006. *Radar Interferometry: Persistent Scatterer Technique*. Springer.

Lanari, R., Mora, O., Manunta, M., Mallorquí, J. J., Berardino, P. and Sansosti, E., 2004. A small baseline approach for investigating deformations on full resolution differential SAR interferograms. *IEEE Trans. Geosci. and Remote Sens.*, 42(7), pp. 1377-1386.

Liu, J., Black, A., Lee, H., Hanaizumi, H. and Moore, J. McM, 2001. Land surface change detection in a desert area in Algeria using multi-temporal ERS SAR coherence images. *Int. J. Remote Sens.*, 22(13), pp. 2463-2477.

Liu, G., Jia, H., Zhang, R., Zhang, H., Jia, H., Yu, B. and Sang, M., 2011. Exploration of subsidence estimation by persistent scatterer InSAR on time series of high resolution TerraSAR-X images. *IEEE J. Sel. Topics Appl. Earth Observ. in Remote Sens*, 4(1), pp. 159-170.

Mittermayer, J., Wollstadt, S., Prats-Iraola, P. and Scheiber, R., 2014. The TerraSAR-X staring spotlight mode concept. *IEEE Trans. Geosci. and Remote Sens.*, 52(6), pp. 3695-3706.

Monserrat, O., Crosetto, M., Cuevas, M. and Crippa, B., 2011. The thermal expansion component of persistent scatterer Interferometry observations. *IEEE Geosci. Remote Sens. Lett.*, 8(5), pp. 864-868.

Osmanoğlu, B., Dixon, T. H., Wdowinski, S., Cabral-Cano, E. and Jiang, T., 2011. Mexico city subsidence observed with persistent scatterer InSAR. *Int. J. Appl. Earth Obs. Geoinf.*, 13, pp. 1-12.

Perissin, D. and Ferretti, A., 2007. Urban target recognition by means of repeated spaceborne SAR images. *IEEE Trans. Geosci. and Remote Sens.*, 45(12), pp. 4043-4058.

Rignot, E. J. M. and van Zyl, J. J., 1993. Change detection techniques for ERS-1 SAR data. *IEEE Trans. Geosci. and Remote Sens.*, 31(4), pp. 896-906.